

Jet measurements at DØ using a k_T algorithm

V. Daniel Elvira^a for the DØ Collaboration.

^aFermi National Accelerator Laboratory, P.O. Box 500, Batavia, IL, 60510-500, USA.

DØ has implemented and calibrated a k_\perp jet algorithm for the first time in a $p\bar{p}$ collider. We present two results based on 1992-1996 data which were recently published: the subjet multiplicity in quark and gluon jets and the central inclusive jet cross section. The measured ratio between subjet multiplicities in gluon and quark jets is consistent with theoretical predictions and previous experimental values. NLO pQCD predictions of the k_\perp inclusive jet cross section agree with the DØ measurement, although marginally in the low p_T range. We also present a preliminary measurement of thrust cross sections, which indicates the need to include higher than α_s^3 terms and resummation in the theoretical calculations.

1. INTRODUCTION

Until recently, only cone algorithms were used to reconstruct jets in $p\bar{p}$ [1] colliders. The cone algorithm used to reconstruct the 1992-1996 Tevatron data [2,3] presents several shortcomings:

- An arbitrary procedure must be implemented to split and merge overlapping calorimeter cones.
- An ad-hoc parameter, R_{sep} [4], is required to accommodate the differences between jet definitions at the parton and detector levels.
- Improved theoretical predictions calculated at the next-to-next-to-leading-order (NNLO) in pQCD are not infrared safe, but exhibit sensitivity to soft radiation.

A second class of jet algorithms, free of these problems, was developed during the past decade [5,6,7]. These recombination algorithms successively merge pairs of nearby objects (partons, particles, or calorimeter towers) in order of increasing relative transverse momentum. A single parameter, D , which approximately characterizes the size of the resulting jets, determines when this merging stops. No further splitting or merging is involved because each object is uniquely assigned to a jet. There is no need to introduce any ad-hoc parameter, because the same

algorithm is applied at the theoretical and experimental level. Furthermore, by design, clustering algorithms are infrared and collinear safe to all orders of calculation.

The DØ Collaboration has implemented a k_\perp algorithm to reconstruct jets from data taken during the 1992-1996 collider run. This paper is a review of the associated measurements recently performed by the DØ experiment [8,9].

2. THE RUN I DØ DETECTOR

DØ is a multipurpose detector designed to study $p\bar{p}$ collisions at the Fermilab Tevatron Collider. A full description of the Run I DØ detector can be found in Ref. [10]. The primary detector components for jet measurements at DØ are the calorimeters, which use liquid-argon as the active medium and uranium as the absorber. The DØ calorimeters provide full solid angle coverage and particle containment (except for neutrinos or high p_T muons), as well as linearity of response with energy and compensation (e/π response ratio is less than 1.05). Transverse segmentation is $\Delta\eta \times \Delta\phi = 0.1 \times 0.1$, with $\eta = -\ln[\tan(\theta/2)]$. The single particle energy resolutions for electrons (e) and pions (π), measured from test beam data, are approximately 15% and 50% respectively.

3. k_{\perp} JET ALGORITHM

The DØ k_{\perp} jet algorithm [8] starts with a list of energy pre-clusters, formed from calorimeter cells, final state partons or particles. The angular separation between pre-clusters is $\Delta\mathcal{R} = \sqrt{\Delta\eta^2 + \Delta\phi^2} > 0.2$.

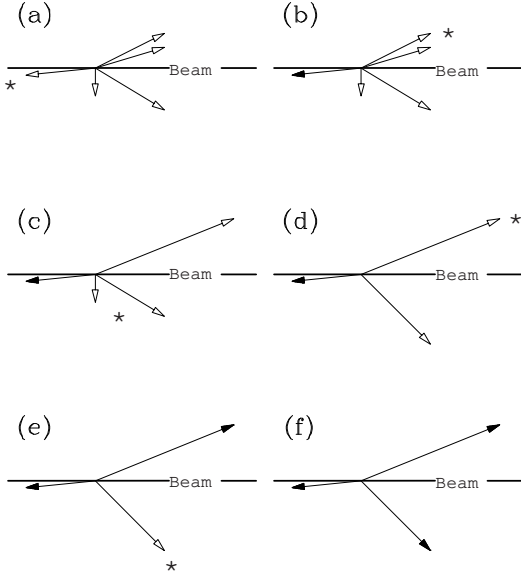


Figure 1. Example of the k_{\perp} merging mechanism on a hard $p\bar{p}$ event. (a) The particles represented by arrows comprise a list of objects. (b-f) Solid arrows represent the final jets reconstructed by the k_{\perp} algorithm, and open arrows represent objects not yet assigned to jets. The five diagrams show successive iterations of the algorithm. In each diagram, an object is labeled as a jet if it is well separated from all other objects. Two objects are merged if they have small relative k_{\perp} . The asterisk labels the relevant objects at each step.

The jet reconstruction is performed in three steps:

1. For each object i in the list, the algorithm defines $d_{ii} = p_{T,i}^2$, where p_T is the momentum transverse to the beam. For each pair (i, j) of objects, it also defines $d_{ij} = \min(p_{T,i}^2, p_{T,j}^2) \frac{\Delta\mathcal{R}_{ij}^2}{D^2}$,

where D is a resolution parameter.

2. If the minimum of all possible d_{ii} and d_{ij} is a d_{ij} , the algorithm replaces objects i and j by their 4-vector sum before going back to step 1. If the minimum is a d_{ii} , then i is defined as a jet and removed from the list of objects.

3. While there is an object left in the list, the algorithm returns to step 1.

The final product of this process is a list of jets, separated by $\Delta\mathcal{R} > D$ from each other. Subjets may be defined by re-running the k_{\perp} algorithm from a list of pre-clusters in a given jet. Pairs of objects with the smallest d_{ij} are merged successively until all remaining d_{ij} satisfy $d_{ij} > y_{\text{cut}} p_{T,\text{jet}}^2$. The resolved objects are called subjets, and the number of subjets within the jet is the subjet multiplicity M . For $y_{\text{cut}}=1$, the entire jet consists of a single subjet ($M=1$). As y_{cut} decreases, the subjet multiplicity increases, until every pre-cluster becomes resolved as a separate subjet in the limit $y_{\text{cut}} \rightarrow 0$.

4. CALIBRATION OF JET MOMENTUM

The uncertainty in the jet energy or momentum is the dominant error in almost every jet measurement at a hadron collider. The jet momentum calibration is described in Ref. [8,11]. The calibration at DØ accounts for detector effects like response, noise, and signal pile-up from previous crossings. It also removes the underlying event formed by the remnant soft partons (u.e.), and the contribution of multiple $p\bar{p}$ interactions. These corrections enter a relation between the momentum of a jet measured in the calorimeter $p_{\text{jet}}^{\text{meas}}$ and the “true” jet momentum $p_{\text{jet}}^{\text{true}}$:

$$p_{\text{jet}}^{\text{true}} = \frac{p_{\text{jet}}^{\text{meas}} - p_O(\eta^{\text{jet}}, \mathcal{L}, p_T^{\text{jet}})}{R_{\text{jet}}(\eta^{\text{jet}}, p^{\text{jet}})} \quad (1)$$

where the offset term p_O corrects for u.e., noise, pile-up, and multiple interactions, while R_{jet} corrects for the response of the calorimeter to jets. The true jet momentum is defined as the particle level jet momentum. A particle level jet is reconstructed from the final state particles, after hadronization but before interaction with the

calorimeter material. The calibration procedure follows closely that of the calibration of the fixed-cone jet algorithm [11].

The fractional momentum resolution for k_\perp jets ($D=1$) is determined from the measured p_T imbalance in dijet events. At 100 (400) GeV, the fractional resolution is $0.061 \pm 0.006 (0.039 \pm 0.003)$. Within statistical and systematic uncertainties, there is not a significant difference between energy resolutions associated with k_\perp ($D=1$) and cone $\mathcal{R}=0.7$ jets.

5. PHYSICS RESULTS

DØ has performed a number of measurements using the k_\perp jet algorithm. These include a study of the structure of quark and gluon jets [8], and measurements of the central ($|\eta| < 0.5$) inclusive jet cross section [9], and thrust distributions.

5.1. Subjet multiplicities

In LO QCD, the fraction of final state jets which are gluons decreases with $x \sim p_T/\sqrt{s}$, the momentum fraction of initial state partons within the proton. For fixed p_T , the gluon jet fraction decreases when \sqrt{s} is decreased from 1800 GeV to 630 GeV. We select gluon and quark enriched samples with identical cuts in events at $\sqrt{s} = 1800$ and 630 GeV to reduce experimental biases and systematic effects. Of the two highest p_T jets in the event, we select k_\perp ($D = 0.5$) jets with $55 < p_T < 100$ GeV and $|\eta| < 0.5$.

There is a simple method to extract a measurement of quark and gluon jets on a statistical basis. If M is the subjet multiplicity in a mixed sample of quark and gluon jets, it may be written as a linear combination of subjet multiplicity in gluon and quark jets:

$$M = f M_g + (1 - f) M_q \quad (2)$$

The coefficients are the fractions of gluon and quark jets in the sample, f and $(1 - f)$, respectively. Consider Eq. (2) for two similar samples of jets at $\sqrt{s} = 1800$ and 630 GeV, assuming M_g and M_q are independent of \sqrt{s} . The solutions are

$$M_q = \frac{f^{1800} M^{630} - f^{630} M^{1800}}{f^{1800} - f^{630}} \quad (3)$$

$$M_g = \frac{(1 - f^{630}) M^{1800} - (1 - f^{1800}) M^{630}}{f^{1800} - f^{630}} \quad (4)$$

where M^{1800} and M^{630} are the experimental measurements in the mixed jet samples at $\sqrt{s} = 1800$ and 630 GeV, and f^{1800} and f^{630} are the gluon jet fractions in the two samples. The method relies on knowledge of the two gluon jet fractions, which are extracted from the HERWIG 5.9[14] Monte Carlo event generator and used in Eqs. (3-4).

Figure 2 shows the average subjet multiplicity ($y_{\text{cut}} = 10^{-3}$) for quark and gluon jets. M_g is significantly larger for gluon jets than for quark jets. The gluon jet fractions are the dominant source of systematic error. We also compute the ratio $R = \frac{\langle M_g \rangle - 1}{\langle M_q \rangle - 1} = 1.84 \pm 0.15(\text{stat})_{-0.18}^{+0.22}(\text{sys})$. Figure 3 shows a comparison between the ratio measured by DØ, the HERWIG 5.9 result of $r=1.91$, the ALEPH[15] value of $r=1.7 \pm 0.1$ (e^+e^- annihilations at $\sqrt{M_Z} = M_Z$), and the associated Monte Carlo and resummation prediction [16]. Good agreement is observed. All of the experimental and theoretical values for r are smaller than the naive QCD prediction value of 2.25 for the ratio of color charges. This is because of higher-order radiation in QCD, which tends to reduce the ratio from the naive value.

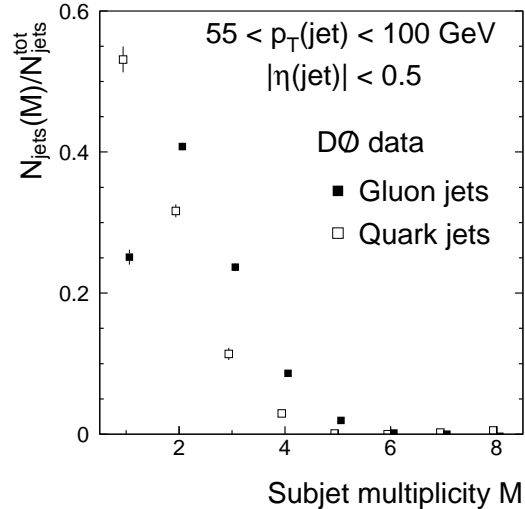


Figure 2. Corrected subjet multiplicity for gluon and quark jets, extracted from DØ data.

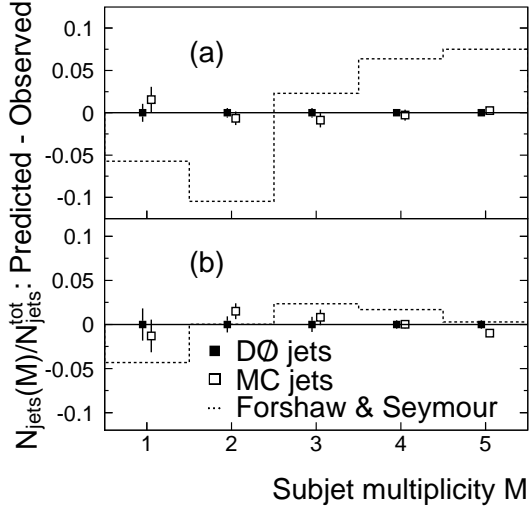


Figure 3. The subjet multiplicity in (a) gluon and (b) quark jets, for DØ data, for the HERWIG Monte Carlo, and resummed predictions.

5.2. Central inclusive jet cross section

The inclusive jet cross section for $|\eta| < 0.5$, $d^2\sigma/(dp_T d\eta)$, was measured as $N/(\Delta\eta\Delta p_T\epsilon L)$, where $\Delta\eta$ and Δp_T are the η and p_T bin sizes, N is the number of jets reconstructed with the k_\perp ($D=1$) algorithm in that bin, ϵ is the overall efficiency for jet and event selection, and L represents the integrated luminosity of the data sample [9].

The fully corrected cross section for $|\eta| < 0.5$ is shown in Fig. 4, along with the statistical uncertainties. The systematic uncertainties include contributions from the jet and event selection, unsmearing, luminosity, and the uncertainty in the momentum scale, which dominates at all transverse momenta. The fractional uncertainties for the different components are plotted in Fig. 5 as a function of the jet transverse momentum.

The results are compared to the NLO pQCD prediction from JETRAD [17], with the renormalization and factorization scales set to $p_T^{\max}/2$, where p_T^{\max} refers to the p_T of the leading jet in an event. The comparisons are made using parameterizations of the parton distribution functions (PDFs) of the CTEQ [18] and MRST [19] families. Figure 6 shows the ratios of (data-theory)/theory. The predictions lie below the

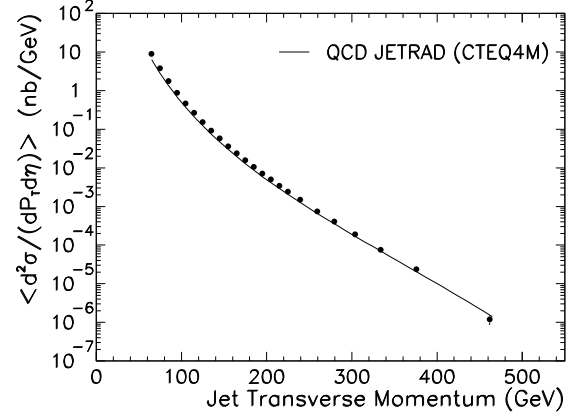


Figure 4. The central ($|\eta| < 0.5$) inclusive jet cross section obtained with the k_\perp algorithm at $\sqrt{s} = 1.8$ TeV. Only statistical errors are included. The solid line shows a prediction from NLO pQCD.

data by about 50% at the lowest p_T and by (10-20)% for $p_T > 200$ GeV. To quantify the comparison in Fig. 6, the fractional systematic uncertainties are multiplied by the predicted cross section, and a χ^2 comparison, using the full correlation matrix, is carried out [2]. Though the agreement is reasonable (χ^2/dof ranges from 1.56 to 1.12, the probabilities from 4 to 31%), the differences in normalization and shape, especially at low p_T , are quite large. The points at low p_T have the highest impact on the χ^2 . If the first four data points are not used in the χ^2 comparison, the probability increases from 29% to 77% when using the CTEQ4HJ PDF.

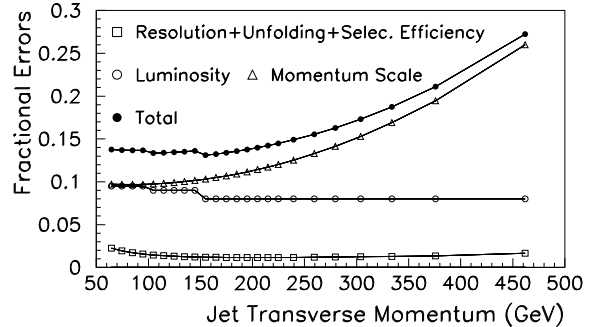


Figure 5. Fractional experimental uncertainties on the cross section.

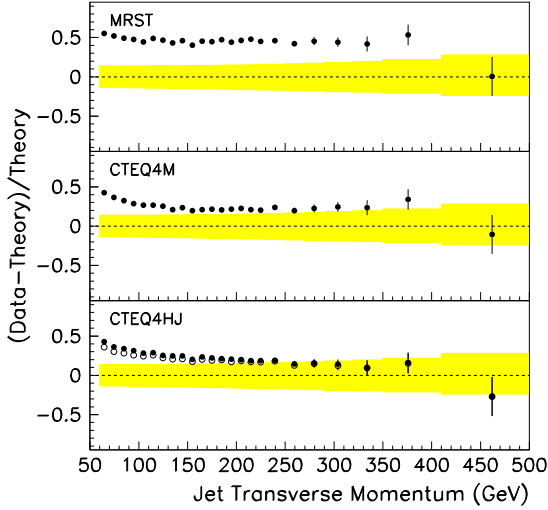


Figure 6. Difference between data and JETRAD pQCD, normalized to the predictions. The shaded bands represent the total systematic uncertainty. In the bottom plot a HERWIG hadronization contribution has been added to the prediction (open circles).

The NLO predictions of the inclusive cross section for k_{\perp} ($D=1$) and cone jets ($\mathcal{R}=0.7$, $R_{\text{sep}}=1.3$) in the same $|\eta| < 0.5$ interval are within a few percent of each other in the p_T range relevant in this analysis [13]. The measured k_{\perp} cross section, however, is 37% (16%) higher than the published cone algorithm [20] at 60 (200) GeV. This difference in the cross sections is consistent with the measured difference in p_T for cone jets matched in η - ϕ space to k_{\perp} jets, as shown in Fig. 7. For the same energy clusters the p_T of k_{\perp} jets ($D=1$) is higher than the E_T of associated cone jets ($\mathcal{R}=0.7$). The difference increases with jet p_T , from about 5 GeV (or 5%) at $p_T \approx 100$ GeV to about 7 GeV (or 3%) at $p_T \approx 250$ GeV [8]. Fig. 7 proves, however, that the energy difference does not depend on the instantaneous luminosity associated with the sample. After offset subtraction, it is clear that k_{\perp} jets are not contaminated by energy coming from pile-up, uranium noise, or multiple interactions.

The effect of final-state hadronization on re-

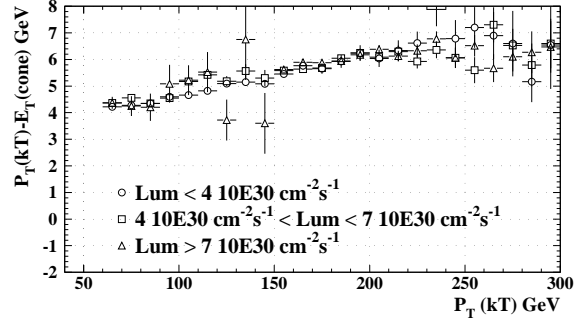


Figure 7. p_T of k_{\perp} jets ($D=1$) minus E_T of the associated cone jets ($\mathcal{R}=0.7$) for samples taken at different instantaneous luminosities.

constructed energy, which might account for the discrepancy between the observed cross section using k_{\perp} and the NLO predictions at low p_T , and also for the difference between the k_{\perp} and cone results, was studied using HERWIG (version 5.9) simulations. Figure 8 shows the ratio of p_T spectra for particle-level to parton-level jets, for both the k_{\perp} and cone algorithms. Particle cone jets, reconstructed from final state particles (after hadronization), have less p_T than the parton jets (before hadronization), because of energy loss outside the cone.

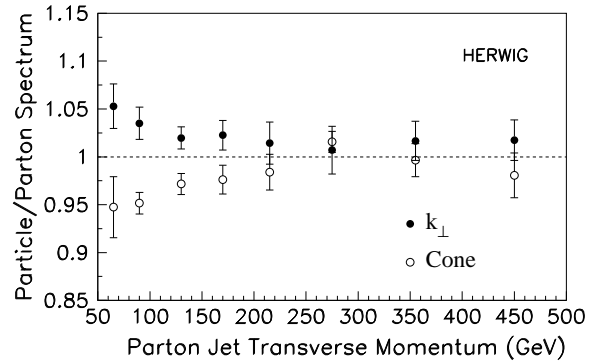


Figure 8. Ratio of particle-level over parton-level HERWIG p_T spectra for jets, as a function of the parton jet transverse momentum.

In contrast, k_{\perp} particle jets are more energetic than their progenitors at the parton level, due to the merging of nearby partons into a single particle jet. Including the hadronization effect derived from HERWIG in the NLO JETRAD predic-

tion improves the χ^2 probability from 29% to 44% (31% to 46%) when using the CTEQ4HJ (MRST) PDF.

We have also investigated the sensitivity of the measurement to the modeling of the background from spectator partons through the use of minimum bias events, and found that it has a small effect on the cross section: at low p_T , where the sensitivity is the largest, an increase of as much as 50% in the underlying event correction decreases the cross section by less than 6%.

5.3. Thrust cross sections

Event shape variables have been extensively used in e^+e^- and ep collider experiments to study the spatial distribution of hadronic final states, to test the predictions of perturbative QCD, and to extract a precise value of the coupling constant α_s . Over the last few years, they have attracted considerable interest, as they have proved to be a fruitful testing ground for recent QCD developments like resummation calculations and non-perturbative corrections.

There are several observables which characterize the shape of an event. To be calculable by perturbation theory, these quantities must be infrared safe, *i.e.* insensitive to the emission of soft or collinear gluons. A widely used variable that meets this requirement is the thrust, defined as

$$T = \max_{\hat{n}} \frac{\sum_i |\vec{p}_i \cdot \hat{n}|}{\sum_i |\vec{p}_i|} \quad (5)$$

where the sum is over all partons, particles or calorimeter towers in the event. The unit vector \hat{n} that maximizes the ratio of the sums is called the thrust axis. The values of thrust range from $T=0.5$ for a perfectly spherical event, to $T=1$ for a pencil-like event, when all emitted particles are collinear. In this latter case, the thrust axis lies along the direction of the particles.

In most of the kinematic range, e^+e^- and ep collider experiments [21] report good agreement of event shape distributions with $O(\alpha_s^2)$ pQCD corrections to the lowest order QED diagram that governs the interaction. Fixed order QCD calculations, however, fail when two widely different energy scales are involved in the event, leading to the appearance of large logarithmic terms at all

orders in the perturbative expansion [22]. This happens in the limit of the two jet back-to-back configuration, when $T \rightarrow 1$. This case is handled by the resummation technique, which identifies the large logarithms in each order of perturbation theory and sums their contributions to all orders. DELPHI reports excellent agreement of thrust distributions in $Z \rightarrow$ hadrons once resummation and hadronization corrections are added to the $O(\alpha_s^2)$ QCD prediction [23].

In a hadron collider, it is convenient to introduce “transverse thrust”, T^T , a Lorenz invariant quantity under z -boosts, which is obtained from Eq. 5 in terms of transverse momenta:

$$T^T = \max_{\hat{n}} \frac{\sum_i |\vec{p}_{T_i} \cdot \hat{n}|}{\sum_i |\vec{p}_{T_i}|} \quad (6)$$

Transverse thrust ranges from $T^T=1$ to $T^T=2/\pi$ ($\langle |\cos \theta| \rangle$) for a back-to-back and an isotropic distribution of particles in the transverse plane, respectively. To minimize systematics associated with the busy environment in a $p\bar{p}$ collider, we use only the two leading jets in the event, reconstructed with a k_{\perp} $D=1$ algorithm, rather than using all calorimeter towers. Other particles in the event are inferred from the angular distribution of the two leading jets.

The measurement of the dijet transverse thrust, T_2^T presents a good opportunity to test resummation models, as well as the recently developed NLO pQCD three-jet generators [24,26]. T_2^T is binned in terms of H_{T3} , defined as the scalar sum of the transverse momenta of the three leading jets of the event $p_{T1} + p_{T2} + p_{T3}$. H_{T3} is an estimator of the energy scale of the event. The lowest order at which pQCD does not give the trivial result $T_2^T=1$ is $O(\alpha_s^3)$, corresponding to up to three parton jets in the final state. A $O(\alpha_s^3)$ calculation, like JETRAD, does not cover the whole physical range of T_2^T . A $O(\alpha_s^3)$ prediction will also fail at $T_2^T \rightarrow 1$, where soft radiation in dijet events contribute large logarithms which need to be resummed.

Figures 9 and 10 show thrust cross sections as a function of $1 - T_2^T$ for the lowest and highest H_{T3} bins: 160-260 GeV and 430-700 GeV.

The error bars are statistical, and the systematic uncertainties are in the 15-30% range. The

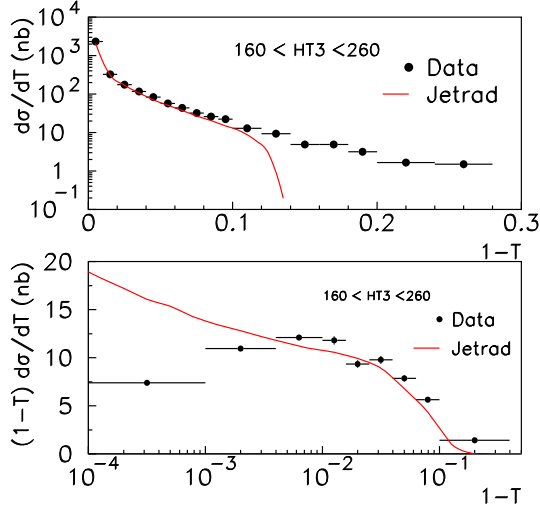


Figure 9. Thrust cross section as a function of $1 - T_2^T$ for the lowest H_{T3} bin: 160-260 GeV.

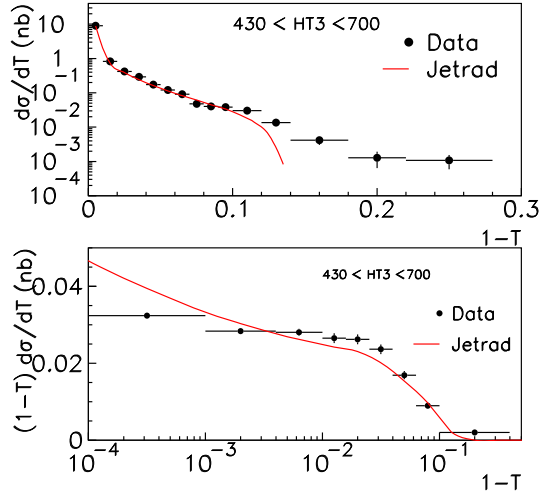


Figure 10. Thrust cross section as a function of $1 - T_2^T$ for the highest H_{T3} bin: 430-700 GeV.

higher the value of $1 - T_2^T$, the more dominant is the contribution of high order terms in α_s . This explains the disagreement between the data and the α_s^3 prediction JETRAD in the high $1 - T_2^T$ range. For example, for T_2^T between $\sqrt{2}/2$ and $\sqrt{3}/2$, the α_s^4 terms contribute to LO. When we expand the range of thrust around unity using a logarithmic scale, we verify that JETRAD also fails, suggesting the need to resum higher order terms to improve agreement. Table 1 displays the agreement probability between the DØ data and JETRAD, which decreases sharply as we incorporate data points in the high and low $1 - T_2^T$ range. The probabilities are calculated using the full covariance error matrix in a χ^2 test.

Table 1

Agreement probability between the DØ data and JETRAD, using the full covariance error matrix in a χ^2 test.

$1 - T_2^T$ Range	χ^2	# d.o.f.	Prob.(%)
0 – 0.1	10	10	42
0 – 0.12	13	11	30
0 – 0.14	42	12	0.004
$10^{-2.4} - 0.063$	2.7	5	75
$10^{-3} - 0.063$	3.8	6	71
$10^{-4} - 0.063$	95	7	0

6. Conclusions

DØ has successfully implemented and calibrated a k_\perp jet algorithm in a $p\bar{p}$ collider. Quark and gluon jets have a different structure consistent with the HERWIG prediction and previous experimental results from $e^+ - e^-$ colliders. The thrust cross section measurements indicate the need to include higher than α_s^3 terms and resummation in the theoretical predictions. They also offer an excellent opportunity to test the recently developed NLO three jet generators [24,26]. The marginal agreement between the measurement of the particle level inclusive k_\perp jet cross section with the α_s^3 theory is opening a debate on mat-

ters such as hadronization, underlying event, and algorithm definition.

REFERENCES

1. J. Huth *et al.*, in *Proc. of Research Directions for the Decade, Snowmass 1990*, edited by E.L. Berger (World Scientific, Singapore, 1992).
2. B. Abbott *et al.* (DØ Collaboration), Phys. Rev. **D64**, 032003 (2001).
3. T. Affolder *et al.* (CDF Collaboration), Phys. Rev. **D64**, 032001 (2001).
4. S.D. Ellis, Z. Kunszt and D.E. Soper, Phys. Rev. Lett. **69**, 3615 (1992).
5. S. Catani, Yu.L. Dokshitzer, M.H. Seymour, and B.R. Webber, Nucl. Phys. **B406**, 187 (1993).
6. S. Catani, Yu.L. Dokshitzer, and B.R. Webber, Phys. Lett. **B285**, 291 (1992).
7. S.D. Ellis and D.E. Soper, Phys. Rev. **D48**, 3160 (1993).
8. V.M. Abazov *et al.* (DØ Collaboration), Phys. Rev. **D65**, 52008 (2002).
9. V.M. Abazov *et al.* (DØ Collaboration), Phys. Rev. Lett. **525**, 221 (2002).
10. S. Abachi *et al.* (DØ Collaboration), Nucl. Instrum. Methods in Phys. Res. **A338**, 185 (1994).
11. B. Abbott *et al.* (DØ Collaboration), Nucl. Instrum. Meth. **A424**, 352 (1999).
12. W. Giele *et al.* (Jet Physics Working Group), in *QCD and Weak Boson Physics in Run II*, edited by U. Baur, R.K. Ellis, D. Zeppenfeld (Fermilab, Batavia, IL, 2000).
13. S. Grinstein, Ph.D. thesis, Univ. de Buenos Aires, Argentina, 2001 (in preparation).
14. G. Marchesini, B.R. Webber, G. Abbiendi, I.G. Knowles, M.H. Seymour, and L. Stanco, Comp. Phys. Comm. **67**, 465 (1992).
15. D. Buskulic *et al.* (ALEPH Collaboration), Phys. Lett. **B346**, 389 (1995).
16. M.H. Seymour, Phys. Lett. **B378**, 279 (1996).
17. W.T. Giele, E.W.N. Glover, and D.A. Kosower, Phys. Rev. Lett. **73**, 2019 (1994).
18. H.L. Lai *et al.*, Phys. Rev. **D55**, 1280 (1997).
19. A. D. Martin *et al.*, Eur. Phys. J. C **4**, 463 (1998).
20. B. Abbott *et al.* (DØ Collaboration), Phys. Rev. Lett. **86**, 1707 (2001).
21. ALEPH Collaboration, D. Decamp *et al.*, Phys. Lett **B234**, 399 (1990); Phys. Lett **B255**, 623 (1991). DELPHI Collaboration, P. Aarnio *et al.*, Phys. Lett. **B240**, 271 (1990). L3 Collaboration, B. Adeva *et al.*, Phys. Lett. **B237**, 136 (1990) OPAL Collaboration, M.Z. Akrawy *et al.*, Phys. Lett. **B235**, 389 (1990); Z. Phys. **C47**, 505 (1990). TASSO Collaboration, W. Bartel *et al.*, Z.Phys. **C33**, 187 (1990).
22. OPAL Collaboration, K. Ackerstaff *et al.*, Z.Phys. **C75**, 193 (1997). DELPHI Collaboration, P. Abreu *et al.*, Z.Phys. **C73**, 229 (1997). H1 Collaboration, C. Adloff *et al.*, Phys.Lett. **B406**, 256 (1997). K. Rabbertz and U. Wollmer hep-ex/0008006; G. J. McCance hep-ex/0008009; G.P.Korchemsky and S.Tafat hep-ph/0007005; Y. Dokshitzer hep-ph/9911299; O. Biebel, P. Movilla and S. bethke, Phys.Lett. **B459**, 326 (1999); S. Catani, L. Trentadue, G. turnock and B. Webber Phys.Lett. **B263**, 491 (1991); G.P.Korchemsky and G.Sterman, Nucl.Phys. **B555**, 335 (1999).
23. DELPHI Collaboration, P. Abreu *et al.*, Z.Phys. **C59**, 21 (1993).
- 24.
25. W.T. Giele and W.B. Kilgore, Phys. Rev. **D55**, 7183 (1997); W. Kilgore, W. Giele, ICHEP 2000, Osaka, Japan (hep-ph/0009193).
26. Z. Nagy, Phys. Rev. Lett. **88**, 122003 (2002).